ACS Catalysis

Article

Effective Control of Particle Size and Electron Density of Pd/C and Sn-Pd/C Nanocatalysts for Vanillin Production *via* Base-Free Oxidation

Weixiao Sun, Shipeng Wu, Yaowei Lu, Yongxing Wang, Qiu-E Cao, and Wenhao Fang

ACS Catal., **Just Accepted Manuscript** • DOI: 10.1021/acscatal.0c01849 • Publication Date (Web): 15 Jun 2020

Just Accepted

is published by the American Chemical Society. 1155 Sixteenth Street N.W., Washington, DC 20036

Effective Control of Particle Size and Electron Density of Pd/C and Sn-Pd/C Nanocatalysts for Vanillin Production *via* Base-Free Oxidation

Weixiao Sun,[†] *Shipeng Wu,*[†] *Yaowei Lu,*[†] *Yongxing Wang,*[†] *Qiue Cao,*[†,‡] *and Wenhao Fang*[†,‡,*]

[†]School of Chemical Science and Technology, Key Laboratory of Medicinal Chemistry for Natural Resource - Ministry of Education, Functional Molecules Analysis and Biotransformation Key Laboratory of Universities in Yunnan Province, 2 North Cuihu Road, Kunming 650091, China

[‡]National Demonstration Center for Experimental Chemistry and Chemical Engineering Education, Yunnan University, Kunming 650091, China

Keywords

selective oxidation, Pd nanoparticles, structure-sensitive reaction, electronic promotor, tin dioxide, vanillin

Abstract

Effective control of particle size and electron density of metal active sites is challenging yet important for supported nanoparticles, as size effect and promotor effect play vital roles in heterogeneous catalysis in nanoscale. In this work, we reported Pd/C and Sn-Pd/C nanocatalysts for the base-free aerobic oxidation of vanillyl alcohol to vanillin, a challenging reaction not only in the fundamental research of selective oxidation of alcohols but also for the practical transformation of bio-based alcohols to value-added chemicals. We effectively tuned the mean size of Pd nanoparticles from 1.8 to 6.7 nm by varying the temperature used for catalyst preparation and further modified the electron density of Pd/C catalyst by adding SnO_2 promotor with different loadings. TEM, HAADF-STEM, XPS, CO chemisorption, and *in situ* DRIFT-IR of CO adsorption

characterizations allowed us to give insight into the unique catalytic property of Pd nanocatalysts. It was conjectured that the base-free aerobic oxidation of vanillyl alcohol to vanillin over Pd/C catalyst can be a structure-sensitive reaction and Pd particle size was decisive for the dispersion of Pd, the proportion of catalytically active Pd^0 sites and intrinsic turn over frequency (*i*TOF). The 1 wt% Pd/C (1.8 nm) catalyst showed an *i*TOF of 268 h^{-1} and 100% yield to vanillin under 120 °C, 5 bar O_2 and 20 mg catalyst within 9 h. We further demonstrated that Sn^{4+} ions in SnO_2 as electronic promoter can promote Pd/C activity by formation of highly active electron-sufficient Pd^0 sites which significantly lowered the apparent activation energy of reaction. The 0.1Sn-Pd/C catalyst showed a higher *i*TOF of 458 h^{-1} and a yield of 100% to vanillin at 120 °C, 3 bar O_2 and 15 mg catalyst within 6 h. Moreover, we verified a satisfying reusability and an adequate substrate scope over the 0.1Sn-Pd/C catalyst.

1. Introduction

Selective oxidation of alcohols into aldehydes or ketones stands out a class of essential and important transformations in organic synthesis and fine-chemical industry.[1, 2] Specifically, oxidation of bio-alcohols derived from lignocellulose would benefit the utilization of renewable organic carbon feedstock parallel to fossil fuels.[3-7] This plays a crucial role in sustainable development and long-term economic stability. Vanillin (4-hydroxy-3-methoxybenzaldehyde) is most often used as a simplified model for the study of lignin conversion, because it features the characteristic structural unit of lignin but offers the easier analytical methodology compared to the complexity of lignin moiety.[8-10] Moreover, production of high-valued vanillin in a rapidly-growing demand is very important to food, pharmaceutical, cosmetic and fine-chemical industries.

Catalytic aerobic oxidation of vanillyl alcohol (4-hydroxy-3-methoxybenzyl alcohol) to

vanillin, as shown in **Scheme 1**, can be really a cost-effective approach only if highly active and selective heterogeneous catalyst is developed. In fundamental research, Mn-,[11, 12] Co-,[13, 14] and Cu-based[15, 16] oxides and their mixed oxides as non-precious catalysts have been intensively studied. Nonetheless, most of those catalysts could only afford dissatisfying conversion of vanillyl alcohol or selectivity of vanillin. What's more, mandatory addition of over-equivalent soluble base (*e.g.*, NaOH) and gas-fill of high-pressured oxidant (*e.g.*, ≥ 20 bar O_2/air) would eventually hamper the green footprint of this process. It is well known that supported noble metal nanoparticles have been widely used as performant catalysts for alcohol oxidations.[1, 2] Even if Pt/C[17] and Pt/MOF-5[18] were described in literature to catalyze the oxidation of vanillyl alcohol with assistant of 1.25 equiv. of NaOH, rather low TOF of 5 h^{-1} and 19 h^{-1} was obtained, respectively. In fact, till date very few noble-metal heterogeneous catalysts have been reported for vanillin production *via* base-free oxidation (**Table 1**). Earlier, a Pt/CuClP ($[PtCl_4]^{2-}$ supported porous copper chlorophosphate framework) catalyst was devised and afforded a low conversion (32%) of vanillyl alcohol at 77% selectivity to vanillin at 170 °C, 20 bar O_2 and 50 mg catalyst within 10 h.[19] Recently, a Au-Pd@HT-PO_4^{3-} (Au-Pd bimetallic nanoparticles on phosphorylated hydrotalcite) photocatalyst was reported, which demonstrated optimally 53% conversion and 50% selectivity under air and visible light with 50 mg catalyst within 24 h.[20] On light of that, the rational design of more efficient heterogeneous catalyst based on noble metals is definitely desirable for vanillin production from selective oxidation.

Carbon materials supported Pd nanoparticles (Pd/C) are highly recognized as model catalyst for liquid-phase alcohol oxidations.[21-24] The size of Pd nanoparticles is generally believed to be one of the most interesting and pivotal factors in determining the performances of Pd/C catalysts.[25-32]

Although many efforts have been devoted to the size-controlled synthesis of Pd/C catalyst, this area remains much challenging. In literature, the size distribution and mean size of Pd/C catalysts can be controlled by various strategies, such as varying the reducing agents and conditions,[25, 28, 32] tuning concentrations of protective agent, Pd salt and precipitant,[27-30] using different carbonaceous materials as support,[26] and changing the preparation temperature.[31] However, most of all the above-mentioned studies on the size effect of Pd/C catalysts dealt with hydrogenation or dehydrogenation reactions. Only one report investigated the size-dependent electrochemical property of different Pd/C nanocatalysts (3.9, 5.2, 6.1 and 7.5 nm) and the Pd nanoparticle with a mean size of 6.1 nm showed the highest formic acid oxidation activity.[27] In fact, studies on the size effect of Pd-catalyzed alcohol oxidations are unexpectedly scarce.[33-35] Further studies are encouraged to help understand in-depth the size effect in Pd nanoparticles-catalyzed aerobic oxidation of alcohols.

On the other hand, introducing a foreign non-precious metal to the active Pd sites is another potential approach to tailor the catalytic property of Pd/C catalyst. In literature, Sn were used as electronic promoter to Pd/C,[36, 37] Pd/SiO_2,[38, 39] and Pd/Al_2O_3 catalysts.[40] Especially for hydrogenation reactions,[36-38, 40] well-dispersed Sn species in the active Pd phase were illustrated to influence the electronic structure of active site, stabilize surface atoms in certain valence state, and tune the chemical binding of the adsorbates. In particular for Pd/C catalysts,[36, 37] Sn promoter was considered to probably modify the Pd sites both geometrically and electronically. But for alcohol oxidation reactions over Sn-promoted Pd/C catalyst, some important fundamentals such as the variations in valence state of metals, the surface atom rearrangement and the reaction kinetics remained entirely unknown.

To the best of our knowledge, there has been no report on the size effect and Sn-promoter effect of Pd/C catalyst for aerobic oxidation of alcohol. Herein, we explored Pd/C as heterogeneous catalyst for the base-free aerobic oxidation of vanillyl alcohol to vanillin. We intended to manipulate the catalytic activity of Pd/C by tuning the Pd particle size and the Pd electron density. The effective experimental methodology, rational catalytic tests and comprehensive catalyst characterizations provided us interesting but solid results that would open discussions on the size effect and promoter effect in nanoscaled heterogeneous catalysis for Pd/C and Sn-Pd/C catalysts.

2. Experimental section

The details of catalyst preparations, characterizations, and catalytic reaction can be found in the supporting information.

3. Results and discussion

3.1 Screening active noble metals and optimizing catalyst pre-reduction

To screen the active noble metals, some typical candidates for liquid-phase oxidation reactions including Ru, Rh, Pd, Pt and Au were first examined for base-free aerobic oxidation of vanillyl alcohol under 120 °C and 5 bar O_2 (**Figure 1a**). 1 wt% noble metal is shown effectively loaded on activated carbon using the given method at 25 °C (**Table S1**). All the prepared catalysts display high specific surface areas (579–624 m^2 g^{-1}) due to the employed carbon material that comprises abundant small slit-shaped pores, as already reported in our previous work. And this bare carbon support is found inactive. Pd/C and Pt/C catalysts show an excellent selectivity (100%) to vanillin but Pd/C is much more active (conv.: 83% *vs*. 36%). Neither vanillic acid nor guaiacol as common by-product is formed. Au/C and Ru/C catalysts afford not only low conversions (*ca.* 20–30%) of vanillyl alcohol but also formation of some unknown by-products, while Rh/C is found barely

active. Therefore, Pd/C-25 catalyst among all the candidates demonstrates a much higher productivity (71 $g^{-1}\cdot h^{-1}\cdot g^{-1}$) toward vanillin.

Following that, pre-reduction of Pd/C-25 catalyst was investigated by using different reduction temperatures in H_2 or various reducing agents (**Figure 1b**). Independent of reduction treatment, the selectivity to vanillin over a series of Pd/C-25 catalysts all reaches 100% without formation of any by-product. Pre-treatment of catalyst in H_2 flow is superior over either a reflux in ethylene glycol at 140 °C or an *in situ* reduction with freshly-made $NaBH_4$ solution. The latter two methods lead obviously to lower conversions of vanillyl alcohol, *i.e.*, 59% and 49%, respectively. As expected, reduction temperature in H_2 could further affect the activity of Pd/C-25 catalyst. Pre-reducing the catalyst at 250 °C is found in this work the most suitable out of 250–450 °C and this range is usually applied for pre-reducing Pd/C catalyst. The variation of catalytic activity over Pd/C-25 due to different pre-reductions can be probably associated with the dispersion and valence state of Pd nanoparticles and interaction between Pd and activated carbon. These features in fact have been well recognized for supported-Pd catalysts to strongly impact their performances in oxidation reactions. In such a context, toward a high production of vanillin from aerobic oxidation of vanillyl alcohol the roles of particle size and electron density of Pd/C catalysts are further tuned and elucidated.

3.2 Tuning particle size of Pd/C catalyst

In this work, Pd particle size was tuned by varying the temperature used during catalyst preparation, specifically from 0 °C to 100 °C with a gap of 25 °C. Previously this strategy was applied successfully to the size-controlled synthesis of supported Au nanoparticles[41, 42] and recently to Pd.[31] It is clearly shown by TEM images that both size distribution and mean size of Pd

nanoparticles can be effectively controlled (**Figure 2**). Pd nanoparticles are observed highly dispersed on carbon support without sintering. The estimated mean size of Pd nanoparticles is found sensitive to the preparation temperature. The mean Pd size gradually grows from 1.8 nm up to 6.7 nm which is confined to a narrow size distribution of *ca.* 4 nm when increasing the preparation temperature from 0 °C to 100 °C (**Figure 3a**). The smallest mean size as low as 1.8 nm can be obtained at 0 °C and such morphology of the Pd/C-0 catalyst is further confirmed by HAADF-STEM (Figure 2). Moreover, the high resolution TEM images randomly collected from different regions on the Pd/C-0 catalyst imply a truncated cubo-octahedral morphology for Pd nanoparticle and show the most exposed facet to be the (111) plane for Pd nanoparticle, which has been widely accepted as the most reactive site of Pd for alcohols oxidation.[43]

Following that, the Pd dispersion can be estimated by using an empirical relationship between particle distribution (D) and mean particle size (d), *i.e.*, $D = 1.12/d \times 100\%$, when a spherical model is assumed for Pd nanoparticles. Meanwhile the Pd dispersion is directly measured by CO chemisorption. As plotted in Figure 3a, the Pd dispersion apparently decreases from *ca.* 60% down to *ca.* 16% with increasing Pd size. Moreover, the estimated Pd dispersions from TEM are found very close to the values determined by CO chemisorption. This reveals the successful control of Pd particle size and the reliable size statistics by TEM. The valence state of supported Pd nanoparticles was analyzed by XPS. The deconvoluted spectra of Pd 3d core level exhibit the co-presence of metallic Pd^0 and cationic Pd^{2+} on catalyst surface (**Figure 3b**). In the Pd $3d_{5/2}$ region Pd^0 species present characteristic BE located at 335.6–335.8 eV while Pd^{2+} species present typical BE located at 337.3–337.6 eV,[30, 44, 45] as listed in **Table S2**. The portion of $Pd^0/(Pd^0 + Pd^{2+})$ goes slowly down from 64% to 52% when Pd particle size grows (Figure 3a). In addition, the BE shifts to higher

values with decreasing Pd particle size, *i.e.*, the BEs of Pd $3d_{5/2}$ obtained from 6.7 nm to 1.8 nm nanoparticles shift from 335.6 eV to 335.8 eV (Table S2, Entries 1–5). This is consistent with the variation of BEs of metallic Pd from a series of Pd/XC-72 catalysts, the declining trend of Pd mean size (8.7 nm to 2.7 nm) led to an increase of BE (335.4 eV to 335.8 eV).[44] And the Pd/C-0 catalyst shows the highest Pd^0 portion and BE at the same time. This phenomenon based on the reduced Pd size can reflect an increase in the density of state near the Fermi level, which may probably enhance the interaction between the Pd surface atoms and adsorbed oxygen molecules.[44] The observed electron deficiency on the smaller Pd nanoparticles is likely attributed to the particle size effect and the strong interaction between Pd and carbon support.[30] Further analysis on C and O from carbon support provides additional information. C 1s spectra can be deconvoluted into four peaks that can be assigned to carbon species in C–C (*ca.* 284.4 eV) of graphite, C–O (*ca.* 285.8 eV) of phenolic, hydroxyl or ether groups, C=O (*ca.* 287.0 eV) of carbonyl or quinone groups, and COO (*ca.* 289.5 eV) of carboxyl group,[46, 47] respectively (**Figure S1**). Meanwhile, deconvolution of O 1s region leads also to four peaks that can be ascribed to oxygen atoms in carbonyl group in quinone (*ca.* 530.9 eV), hydroxyl group (*ca.* 532.1 eV), non-carbonyl (ether-type) group (*ca.* 533.4 eV), and carboxyl group (*ca.* 535.3 eV),[48] respectively (Figure S1). Thus the identification of C 1s and O 1s bands is well consistent. These BEs appear independent of Pd particle size. Therefore, the surface of activated carbon that is used as support in this work is functionalized by various O-containing groups. And the hydroxyl, carbonyl and quinone groups bonding to carbon surface has been disclosed highly essential to facilitate the adsorption and activation of OH group during base-free oxidations.[49, 50]

As displayed in **Figure 3c**, a size effect of Pd can be observed on conversion of vanilly alcohol

whereas selectivity to vanillin is independent on Pd size, maintaining 100%. Conversion declines from 90% to 52% when Pd size grows from 1.8 nm up to 6.7 nm. This effect is also detectable for productivity of vanillin, *i.e.*, from 77 $g^{-1}\cdot h^{-1}\cdot g^{-1}$ to 44 $g^{-1}\cdot h^{-1}\cdot g^{-1}$. Deeper analysis on the kinetic-controlled region reveals that the initial reaction rate of vanillyl alcohol is sensitive and strongly depends on Pd size, which declines steeply from 4.17 $\mu mol\cdot g^{-1}\cdot s^{-1}$ to 0.89 $\mu mol\cdot g^{-1}\cdot s^{-1}$. In fact, the intrinsic activity of Pd/C catalyst is rationally determined by the surface reactive Pd atoms. Thereby, the *i*TOF based on the Pd dispersion from CO chemisorption and the initial reaction rate is calculated and plotted against the Pd size in **Figure 3d**. It can be speculated that base-free aerobic oxidation of vanillyl alcohol to vanillin over Pd/C catalyst is probably a structure-sensitive reaction, *i.e.*, an increase in Pd size brings about a continuous decrease in the *i*TOF. Specifically when Pd size grows from 1.8 nm to 6.7 nm the *i*TOF significantly declines from 268 h^{-1} to 185 h^{-1}. The Pd/C-0 (*d*: 1.8 nm) catalyst shows the highest *i*TOF and 100% yield to vanillin can be obtained under 120 °C, 5 bar O_2 and 25 mg catalyst within 9 h. Further inspection on the geometry of a Pd atom may provide an insight into the nature of Pd size effect. Typically, a Pd nanoparticle consists of terrace, edge and corner Pd atoms, which have higher (terrace atoms) and lower (edge and corner atoms) coordination numbers. It has been shown for supported metal nanoparticles which present truncated cubo-octahedral geometric structure that the proportions of edge and corner atoms may depend on approximately d^{-2} and d^{-3} of the mean particle size (d) while the relation for terrace atoms may be about d^{-1}.[51] These correlations can be slightly altered on the basis of different atomic radius and geometries. Hence, the fractions of different Pd atomic sites for Pd/C catalysts bearing different sizes are calculated and plotted in Figure 3d. The fraction of coordinatively unsaturated Pd atoms (*i.e.*, edge and corner atoms) obviously increases from 3% up to 38% by decreasing Pd

particle size, and this tendency seems more pronounced when the Pd size is lower than 3.5 nm. Meanwhile the fraction of coordinatively saturated Pd atoms (*i.e.*, terrace atoms) fluctuates gently within *ca.* 17%–23%. It is well known that different coordination numbers of metal atoms can lead to different catalytic activities. The edge and corner atoms are most often more active than terrace atoms in structure-sensitive reactions. As shown in Figure 3d, the declining trend of *i*TOF for Pd/C catalysts with increasing Pd sizes for base-free aerobic oxidation of vanillyl alcohol roughly follows the declining trend of the fraction of edge and corner atoms. This observation indicates that the coordinatively unsaturated Pd atoms on Pd nanoparticles can probably play vital roles in the catalytic active sites.

3.3 Tuning electron density of Pd/C catalyst by promoter

Thereafter the activity of the Pd/C-0 catalyst was further modified by tuning the electron density of Pd^0 site with a metal promoter (0.1 wt%). In order to avoid any possible saturation in activity, a lower amount of catalyst (15 mg) was used. As reported in **Figure 4a**, Sn enables to promote conversion of vanillyl alcohol by about 45%, *i.e.*, from 69% to 100%. Accordingly, productivity to vanillin rises to 104 $g^{-1}\cdot h^{-1}\cdot g^{-1}$. On the contrary, addition of Bi, Cu, Mn, Co and Zn inhibits the conversion down to the range of 21–54%. Selectivity to vanillin is only determined by Pd/C catalyst but not influenced by the added metals. Hence the loading (0.02–0.5 wt%) of Sn promoter need be investigated. Sn loading measured by ICP-MS is very close to the theoretical values and has no effect on the specific surface areas of *y*Sn-Pd/C catalysts (**Table S3**). As presented in **Figure 4b**, Sn loading can affect the catalytic activity of the Pd/C-0 catalyst. A typical volcano-like relationship can be established between conversion of vanillyl alcohol and promoter loading. The conversion first increases and then decreases by adding Sn. This promotion effect is

only observed when Sn loading is of 0.1–0.2 wt%, and 0.1Sn-Pd/C is found the most active one among *y*Sn-Pd/C catalysts. Notably, the prepared Sn/C catalyst (*i.e.*, Sn(IV)O_2/C) as a reference is inactive. Moreover, Sn/C catalyst was reduced at 450 °C and 600 °C with H_2 respectively, so that Sn(II)O/C and Sn(0)/C can be obtained. Those Sn catalysts show no activity under the same reaction conditions, which can reflect that Pd is the active site.

The main reaction parameters including O_2 pressure and reaction temperature were investigated on the 0.1Sn-Pd/C catalyst. As shown in **Figure S2a**, O_2 pressure slightly influences conversion of vanillyl alcohol. An increase from 91% to 100% is detected under 1–3 bar O_2. Thus a total conversion can be achieved under ambient O_2 pressure by simply adding more catalyst (20 mg). Further increase in O_2 pressure cannot change the activity. And then, the 0.1Sn-Pd/C catalyst shows a strong activity-dependence on reaction temperature (Figure S2b). Conversion of vanillyl alcohol almost linearly rises from 21% to 100% at 90–120 °C. Therefore, the activation of vanillyl alcohol is difficult and a suitable catalyst is essential for high production of vanillin. As compared in the time course test (**Figure 5a**), it can be clearly seen that the addition of Sn promoter allows simultaneously increasing conversion of vanillyl alcohol over the Pd/C-0 catalyst. The conversion rate is significantly accelerated over the 0.1Sn-Pd/C catalyst and 100% yield to vanillin can be already achieved after 6 h, whereas a plateau for vanillin yield of *ca.* 70% is observed in absence of Sn even after 18 h of reaction. To our satisfaction, a much higher *i*TOF value of 458 h^{-1} can be reported on 0.1Sn-Pd/C catalyst. Compared to the ever-reported noble-metal-based catalytic systems (Table 1), our catalysts show superior TON (turnover number) values that are *ca.* 2–8 times higher than the data from literature. Calculation of the apparent activation energy (E_a, the kinetic data and the computational details are shown in **Table S4**) by the numerical regression assuming

valid Arrhenius law further reveals that Sn-promoted Pd/C catalyst is much more active (**Figure 5b**), which presents the lower E_a of 55.6 kJ·mol^{-1}, while Pd/C alone affords the higher E_a of 67.7 kJ·mol^{-1}. This kinetic result is in good agreement with the promoter effect in catalytic performances.

In order to understand in-depth the promoting role of Sn, some more characterizations focusing on the interaction between Pd and Sn were carried out. Bright-field STEM and HAADF-STEM images (**Figure 6a-b**) show a highly analogue morphology for 0.1Sn-Pd/C compared to Pd/C-0. Pd nanoparticles with a mean size of *ca.* 1.8 nm are well dispersed on carbon support and the corresponding size distribution of Pd nanoparticles is found in a narrow range (0.5–4.5 nm). The atomic resolution image for a representative Pd nanoparticle shows a typical truncated cubo-octahedral geometry, in consistent with the modeling used for discussion before. EDS elemental maps present the co-existence of Sn, Pb and C and the locations of Sn and Pd can roughly overlap each other (**Figure 6c-f**). Moreover, the line-scan EDS analysis randomly across several nanoparticles on carbon support shows that Sn and Pd elements are uniformly distributed within all these Sn-Pd nanoparticles (**Figure S3**). These results reveal that Sn atoms can be incorporated into Pd nanoparticles to form Sn-Pd alloy structure, and it indicates that Pd and Sn may interact effectively, leading probably to a strong interaction.

XPS spectra of Pd $3d_{5/2}$ band exhibit two peaks with BEs of *ca.* 335.2–335.5 eV and 337.1–337.3 eV (**Figure 7a**), which can be attributed to typical Pd^0 and Pd^{2+} species,[52, 53] respectively. Sn 3d core level presents two symmetric peaks with BEs of *ca.* 486.4–486.7 eV and 494.9–495.2 eV for Sn $3d_{5/2}$ and $3d_{3/2}$ bands (**Figure 7b**), respectively. These peaks correspond to the characteristic Sn^{4+} species.[54] When Sn loading is lower than 0.1 wt.%, the Sn 3d core level is

not detectable. Compared with the Pd/C-0 catalyst (Table S2), adding Sn leads to lower BEs for Pd^0 species (*i.e.*, a shift of *ca.* 0.3–0.6 eV), which is attributed in literature to the electron transfer from Sn to Pd.[38] Meanwhile the C 1s and O 1s XPS spectra show no obvious variation (Figure S4). As listed in Table S2, when the content of SnO_2 promoter increases from 0.02 to 0.5 wt.%, the BE of Pd^0 shifts lower values (from 335.5 eV to 335.2 eV) and whilst Sn^{4+} to higher values (from 486.4 eV to 486.7 eV). This is consistent with the observed charge transfer between Sn and Pd. Moreover, Sn loading can affect the portion of Pd^0 active sites. A volcano-like tendency can be plotted for the portion of Pd^0 against the Sn loading (Figure 4b). An optimum (66%) is obtained on the 0.1Sn-Pd/C catalyst, and this portion of catalytically active sites is slightly increased (66% *vs* 64%) by SnO_2 promoter. Compared to the BEs of Pd^0 species from the surfaces of Pd-Sn/HBDD,[39] PdSn/P25,[55] and Pd-SnO_2/Al_2O_3 catalysts,[40] the present 0.1Sn-Pd/C catalyst shows a lower BE for Pd^0 species. And moreover, no metallic Sn^0 but only Sn^{4+} species is observed. This reveals the formation of electron-sufficient Pd^0 active sites due to a strong electronic interaction between the 3d orbitals of two metals.[56] The BE shift of Pd^0 species can be attributed to an enhanced charge transfer from Sn to Pd probably assisted by activated carbon support, which may increase the interfacial electron density of Pd atoms and immediately stabilize Sn^{4+} species.

To further elucidate the modification of electronic structure of Pd species by SnO_2 promoter, *in situ* DRIFT-IR spectra of CO adsorption were recorded on the Pd/C-0 and all the *y*Sn-Pd/C catalysts. This technique is sensitive and informative for analyzing only the exposed surface Pd sites, whereas sub-surface or bulk Pd sites cannot be characterized. In addition, CO molecule cannot be adsorbed on Sn.[57] Thereby, this technique would offer straightforward information on the accessible Pd sites in catalytic reactions. As displayed in **Figure 8**, the spectra can be generally

divided into two regions that correspond to adsorption of CO on ionic Pd sites (*ca.* 2100–2200 cm^{-1}) and metallic Pd sites (*ca.* 1800–2100 cm^{-1}),[40, 58] respectively. As the controlled experiment, the unreduced Pd/C-0 and 0.1Sn-Pd/C catalysts show very similar patterns in the spectra. The peaks at 2175 cm^{-1} and 2118 cm^{-1} can be respectively attributed to linearly adsorbed CO on Pd^{2+} and Pd^{+} sites,[58] as expected. The peaks in 2100–2200 cm^{-1} have been assigned to linearly bonded Pd-CO species on discontinuities between planes (*i.e.*, corners and edges).[40] The peak at 2060 cm^{-1} is also related to linear adsorption of CO on Pd (111) defects.[40] The adsorption peak of 0.1Sn-Pd/C slightly shifts to the lower wavenumber, which indicates the electron transfer from Sn to Pd.[55] To our interest, the Pd/C-0 and the *y*Sn-Pd/C catalysts after *in situ* reduction in H_2 at 250 °C (*i.e.*, the same condition used for catalytic reaction) show obviously different spectra *versus* Sn loading. The CO adsorption peaks due to the surface ionic Pd sites (2175 cm^{-1}, 2112 cm^{-1} and 2024 cm^{-1}) of the Pd/C-0 catalyst are found largely reduced with increasing Sn and almost disappear on the 0.1Sn-Pd/C catalyst (only a minor peak at 2107 cm^{-1} is preserved).[58] This observation is in consistent with XPS results. Note that XPS analysis is *ex-situ* conducted and the catalysts exposed to air can be partially reduced on surface. Moreover, it can be clearly seen that the presence of Sn improves the reduction of ionic Pd species. For Pd/C-0 and 0.02Sn-Pd/C catalysts, several CO adsorption peaks in low intensity are recorded, which can be ascribed to linear-bonded CO on Pd (111) defects (2067 cm^{-1}), bridge-bonded CO on Pd (100) plane (1975 cm^{-1}) and Pd (111) plane (1936 cm^{-1}),[40] respectively. The 0.1Sn-Pd/C catalyst also presents the above three peaks. Notably, on this catalyst the CO adsorption on coordinatively unsaturated Pd sites is strengthened. Although SnO_2 cannot adsorb CO, it may enhance the bridge-bonded CO on metallic Pd sites, reflected by much more intense adsorption peaks at 1974 cm^{-1} and 1934 cm^{-1}. This phenomenon indicates an

increased fraction of surface contiguous Pd sites due to the addition of Sn^{4+} ions, which could be associated with the strong promoter effect between Sn and Pd. To be recalled, both linear and bridged adsorptions of CO shift to lower frequency (*ca.* 3 cm^{-1}) upon SnO_2 promoter. These shifts can be probably originated from a remarkable enhancement in *d* orbital electron density due to the electron-transfer from Sn to Pd, which brings about a stronger electronic back-donation to $2\pi^*$ molecular orbitals of CO.[59] More importantly, two new intense adsorption peaks are observed at 1890 cm^{-1} and 1850 cm^{-1} for the 0.1Sn-Pd/C catalyst, which can be attributed to bridged- and multi-bonded CO on metallic Pd ensembles consisted of two or three contiguous Pd atoms.[55, 58, 59] However, these CO adsorption peaks and the corresponding metallic Pd sites become much weaker and even vanished at a higher Sn loading (≥ 0.2%). This phenomenon implies the different surface atom arrangements between Pd and Sn-Pd alloy nanoparticles upon Sn promotor, which is speculated to enhance the adsorption and activation of reactants.

3.4 Stability and reusability

The stability and reusability is important for heterogeneous catalyst due to cost control and practical applications. For this reason the used catalyst after separation and post-treatment is tested in a consecutive recycling experiment. Before that, the reaction mixture was centrifuged at 10,000 rpm for 10 min, the obtained solid catalyst was washed several times by ethanol and water to remove organic compounds adsorbed on catalyst surface followed by a H_2 reduction at 250 °C for 2 h. Both Pd/C-0 and 0.1Sn-Pd/C catalysts are examined. As presented in **Figure S5**, Pd/C-0 catalyst shows a very minor activity loss (*ca.* 8%) after the third cycle but becomes stable afterwards, as compared to the fresh catalyst. This insignificant deactivation can be probably due to the partial leaching of Pd, as ICP-MS reveals that 5.9% Pd species has leached to the reaction mixture. This

phenomenon is most often responsible for Pd/C deactivation in liquid phase reaction.[60] Adsorption of organic compounds on Pd surface or partial oxidation of Pd nanoparticles as possible reasons for the deactivation can be excluded due to the rigorous post-treatment. On the contrary, 0.1Sn-Pd/C catalyst shows a considerable stability during five cycles under the optimized conditions (Figure S5). In order to avoid any false stability due to a saturated catalytic activity, the used catalyst was further tested in the kinetic-controlled region so that the intrinsic activity can be rationally monitored. It is clearly disclosed that 0.1Sn-Pd/C catalyst exhibits indeed an excellent stability and reusability for base-free aerobic oxidation of vanillyl alcohol to vanillin. This can be attributed to an enhanced interaction between Pd and carbon support promoted by surface SnO_2.

3.5 Substrate scope

The 0.1Sn-Pd/C catalyst has demonstrated superior activity and selectivity for base-free selective oxidation of vanillyl alcohol, a complicated model alcohol. This inspires us to further investigate the oxidation performances of this catalyst towards various primary alcohols. The selected alcohols are representatives in the literature to evaluate supported-Pd catalysts under mild conditions. As shown in **Table 2**, the 0.1Sn-Pd/C catalyst can selectively convert a series of alcohols into corresponding aldehydes. High conversions (96−100%) of substrates can be obtained on cinnamyl alcohol (entry 1), cyclohexylmethanol (entry 2) and pyridin-4-methanol (entry 3) at 60 °C and 1 bar O_2. Meanwhile, a few complicated alcohols such as 3,4-(methylenedioxy)benzyl alcohol (entry 4) and 2-naphthalene methanol (entry 5) can be also selectively transformed at moderate conversions, *i.e.*, 78% and 67% respectively. 2-Thiophenemethanol (entry 6) and 1-octanol (entry 7) are much more difficult in activating, as expected, due to the presence of sulfur heteroatom and non-branched aliphatic carbon backbone. Note some bulky esters might be formed

during oxidation of 1-octanol. In short, 0.1Sn-Pd/C is shown as a highly selective catalyst for base-free aerobic oxidation of a wide scope of aromatic alcohol, α,β-unsaturated alcohol, alicyclic alcohol, heterocyclic alcohols bearing heteroatoms, and even linear aliphatic alcohol.

4. Conclusion

In this work, Pd/C catalyst was shown highly active and selective for vanillin production through benign (base-free, low-temperature and low pressure), aerobic oxidation of vanillyl alcohol. In particular, Pd/C as model oxidation catalyst was successfully ameliorated by effective control of particle size and electron density of Pd nanoparticles. The structure-sensitive effect was observed for Pd/C catalyzed base-free aerobic oxidation of vanillyl alcohol. The smaller Pd size was the more active the catalyst can behave. The coordinatively unsaturated Pd atoms located at corner and edge sites on metallic Pd^0 nanoparticles can be considered to mainly determine the intrinsic catalytic activity of Pd species, *i.e.*, initial conversion rate and *i*TOF. Further addition of SnO_2 promoter allowed modifying the electron density of surface Pd^0. Sn^{4+} ions in SnO_2 as electronic promoter were shown well dispersed in the active phase, and enabled to induce the formation of electron-sufficient Pd^0 sites through an enhanced charge transfer from Sn to Pd, which may increase the interfacial electron density of Pd atoms and simultaneously stabilize Sn^{4+} ions. Such highly active sites were found beneficial to significantly lower the apparent activation energy of reaction, and further improved the intrinsic catalytic activity. The developed 0.1Sn-Pd/C (~1.8 nm) catalyst showed a high *i*TOF value (458 h^{-1}) and 100% yield of vanillin under mild conditions, exhibited satisfying catalytic stability and reusability, and finally displayed superior TON values for a wide scope of alcohols in base-free aerobic oxidations.

ASSOCIATED CONTENT

AUTHOR INFORMATION

Corresponding Author

*Email: wenhao.fang@ynu.edu.cn (Wenhao Fang)

Author Contributions

The manuscript was written through contributions of all authors. All authors have given approval to the final version of the manuscript.

Notes

The authors declare no competing financial interest.

Supporting Information

The following files are available free of charge.

Experimental details, elemental analysis, specific surface areas, XPS spectra and parameters, STEM image and the line-scan EDS spectrum, influence of O_2 pressure and reaction temperature, recycling test. (PDF file)

Acknowledgments

This work was supported by National Natural Science Foundation of China (21763031, 21603187), National Special Funds of China (C176220100063), Program for Excellent Young Talents of Yunnan University, Joint Fund of Yunnan Science and Technology Department - Yunnan University (2019FY003003), Scientific and Technological Innovation Team of Green Synthesis and Activity Research of Natural-like Heterocyclic Compounds Libraries in Universities of Yunnan Province.

References

(1) Dimitratos, N.; Lopez-Sanchez, J. A.; Hutchings, G. J., Selective liquid phase oxidation with supported metal nanoparticles. *Chem. Sci.* **2012,** *3*, 20-44.

(2) Guo, Z.; Liu, B.; Zhang, Q.; Deng, W.; Wang, Y.; Yang, Y., Recent advances in heterogeneous selective oxidation catalysis for sustainable chemistry. *Chem. Soc. Rev.* **2014,** *43*, 3480-3524.

(3) Chen, S.; Wojcieszak, R.; Dumeignil, F.; Marceau, E.; Royer, S., How Catalysts and Experimental Conditions Determine the Selective Hydroconversion of Furfural and 5-Hydroxymethylfurfural. *Chem. Rev.* **2018,** *118*, 11023-11117.

(4) Wang, M.; Ma, J.; Liu, H.; Luo, N.; Zhao, Z.; Wang, F., Sustainable Productions of Organic Acids and Their Derivatives from Biomass via Selective Oxidative Cleavage of C–C Bond. *ACS Catal.* **2018,** *8*, 2129-2165.

(5) Wu, S.; Sun, W.; Chen, J.; Zhao, J.; Cao, Q.; Fang, W.; Zhao, Q., Efficient imine synthesis from oxidative coupling of alcohols and amines under air atmosphere catalysed by Zn-doped Al_2O_3 supported Au nanoparticles. *J. Catal.* **2019,** *377*, 110-121.

(6) Gao, T.; Yin, Y.; Zhu, G.; Cao, Q.; Fang, W., Co_3O_4 NPs decorated Mn-Co-O solid solution as highly selective catalyst for aerobic base-free oxidation of 5-HMF to 2,5-FDCA in water. *Catal. Today* **2019,** DOI: 10.1016/j.cattod.2019.03.065.

(7) Gao, T.; Zhang, H.; Hu, C.; Jing, F.; Fang, W., Base-Free Aerobic Oxidation of 5-Hydroxymethylfurfural on Ru(0) Center Cooperated with Co(II)/Co(III) Redox Pair over the One-Pot Synthesized Ru-Co Composites. *Ind. Eng. Chem. Res.* **2020,** DOI: 10.1021/acs.iecr.0c00937.

(8) Augugliaro, V.; Camera-Roda, G.; Loddo, V.; Palmisano, G.; Palmisano, L.; Parrino, F.; Puma, M. A., Synthesis of vanillin in water by TiO_2 photocatalysis. *Appl. Catal. B* **2012,** *111-112*, 555-561.

(9) Hao, P.; Schwartz, D. K.; Medlin, J. W., Effect of Surface Hydrophobicity of Pd/Al_2O_3 on Vanillin Hydrodeoxygenation in a Water/Oil System. *ACS Catal.* **2018,** *8*, 11165-11173.

(10) Fan, R.; Chen, C.; Han, M.; Gong, W.; Zhang, H.; Zhang, Y.; Zhao, H.; Wang, G., Highly Dispersed Copper Nanoparticles Supported on Activated Carbon as an Efficient Catalyst for Selective Reduction of Vanillin. *Small* **2018,** *14*, 1801953.

(11) Jha, A.; Patil, K. R.; Rode, C. V., Mixed Co–Mn Oxide-Catalysed Selective Aerobic Oxidation of Vanillyl Alcohol to Vanillin in Base-Free Conditions. *ChemPlusChem* **2013,** *78*, 1384-1392.

(12) Ramana, S.; Rao, B. G.; Venkataswamy, P.; Rangaswamy, A.; Reddy, B. M., Nanostructured Mn-doped ceria solid solutions for efficient oxidation of vanillyl alcohol. *J. Mol. Catal. A: Chem.* **2016,** *415*, 113-121.

(13) Jha, A.; Rode, C. V., Highly selective liquid-phase aerobic oxidation of vanillyl alcohol to vanillin on cobalt oxide (Co_3O_4) nanoparticles. *New J. Chem.* **2013,** *37*, 2669-2674.

(14) Liang, C.; Ma, Q.; Yuan, H.; Wang, Y.; Mao, J.; Chen, Z.; Yao, J.; Li, H., Aerobic Oxidation of 2-Methoxy-4-methylphenol to Vanillin Catalyzed by Cobalt/NaOH: Identification of $CoO_x(OH)_y$ Nanoparticles as the True Catalyst. *ACS Catal.* **2018,** *8*, 9103-9114.

(15) Saha, S.; Hamid, S. B. A.; Ali, T. H., Catalytic evaluation on liquid phase oxidation of vanillyl alcohol using air and H_2O_2 over mesoporous Cu-Ti composite oxide. *Appl. Surf. Sci.* **2017,** *394*, 205-218.

(16) Saha, S.; Abd Hamid, S. B., $CuZrO_3$ nanoparticles catalyst in aerobic oxidation of vanillyl alcohol. *RSC Adv.* **2017,** *7*, 9914-9925.

(17) Tarasov, A. L.; Kustov, L. M.; Bogolyubov, A. A.; Kiselyov, A. S.; Semenov, V. V., New and efficient procedure for the oxidation of dioxybenzylic alcohols into aldehydes with Pt and Pd-based catalysts under flow reactor conditions. *Appl. Catal. A* **2009,** *366*, 227-231.

(18) Tarasov, A. L.; Kustov, L. M.; Isaeva, V. I.; Kalenchuk, A. N.; Mishin, I. V.; Kapustin, G. I.; Bogdan, V. I., Platinum-containing catalyst supported on a metal-organic framework structure in the selective oxidation of benzyl alcohol derivatives into aldehydes. *Kinet. Catal.* **2011,** *52*, 273-276.

(19) Hinde, C. S.; Ansovini, D.; Wells, P. P.; Collins, G.; Aswegen, S. V.; Holmes, J. D.; Hor, T. S. A.; Raja, R., Elucidating Structure–Property Relationships in the Design of Metal Nanoparticle Catalysts for the Activation of Molecular Oxygen. *ACS Catal.* **2015,** *5*, 3807-3816.

(20) Wu, M.; Pang, J.-H.; Song, P.-P.; Peng, J.-J.; Xu, F.; Li, Q.; Zhang, X.-M., Visible light-driven oxidation of vanillyl alcohol in air with Au–Pd bimetallic nanoparticles on phosphorylated hydrotalcite. *New J. Chem.* **2019,** *43*, 1964-1971.

(21) Lu, A.-H.; Li, W.-C.; Hou, Z.; Schüth, F., Molecular level dispersed Pd clusters in the carbon walls of ordered mesoporous carbon as a highly selective alcohol oxidation catalyst. *Chem. Commun.* **2007**, 1038-1040.

(22) Villa, A.; Wang, D.; Dimitratos, N.; Su, D.; Trevisan, V.; Prati, L., Pd on carbon nanotubes for liquid phase alcohol oxidation. *Catal. Today* **2010,** *150*, 8-15.

(23) Zhang, P.; Gong, Y.; Li, H.; Chen, Z.; Wang, Y., Solvent-free aerobic oxidation of hydrocarbons and alcohols with Pd@N-doped carbon from glucose. *Nat. Commun.* **2013,** *4*, 1593.

(24) Yan, Y.; Chen, Y.; Jia, X.; Yang, Y., Palladium nanoparticles supported on organosilane-functionalized carbon nanotube for solvent-free aerobic oxidation of benzyl alcohol. *Appl. Catal. B* **2014,** *156-157*, 385-397.

(25) Neri, G.; Musolino, M. G.; Milone, C.; Pietropaolo, D.; Galvagno, S., Particle size effect in the catalytic hydrogenation of 2,4-dinitrotoluene over Pd/C catalysts. *Appl. Catal. A* **2001,** *208*, 307-316.

(26) Amorim, C.; Keane, M. A., Palladium supported on structured and nonstructured carbon: A consideration of Pd particle size and the nature of reactive hydrogen. *J. Colloid Interface Sci.* **2008,** *322*, 196-208.

(27) Suo, Y.; Hsing, I. M., Size-controlled synthesis and impedance-based mechanistic understanding of Pd/C nanoparticles for formic acid oxidation. *Electrochim. Acta* **2009,** *55*, 210-217.

(28) Wang, Q.; Cheng, H.; Liu, R.; Hao, J.; Yu, Y.; Zhao, F., Influence of metal particle size on the hydrogenation of maleic anhydride over Pd/C catalysts in $scCO_2$. *Catal. Today* **2009,** *148*, 368-372.

(29) Chinthaginjala, J. K.; Villa, A.; Su, D. S.; Mojet, B. L.; Lefferts, L., Nitrite reduction over Pd supported CNFs: Metal particle size effect on selectivity. *Catal. Today* **2012,** *183*, 119-123.

(30) Li, J.; Chen, W.; Zhao, H.; Zheng, X.; Wu, L.; Pan, H.; Zhu, J.; Chen, Y.; Lu, J., Size-dependent

catalytic activity over carbon-supported palladium nanoparticles in dehydrogenation of formic acid. *J. Catal.* **2017,** *352*, 371-381.

(31) Hong, S.; Hwang, H.; Hwang, J. P.; Kim, J. W.; Lee, C. H.; Lee, J., The effect of morphological difference and hydride incorporation on the activity of Pd/C catalysts in direct alkaline formate fuel cell. *Catal. Today* **2019,** DOI: 10.1016/j.cattod.2019.06.042.

(32) Kim, Y.; Kim, D. H., Understanding the effect of Pd size on formic acid dehydrogenation via size-controlled Pd/C catalysts prepared by $NaBH_4$ treatment. *Appl. Catal. B* **2019,** *244*, 684-693.

(33) Mori, K.; Hara, T.; Mizugaki, T.; Ebitani, K.; Kaneda, K., Hydroxyapatite-Supported Palladium Nanoclusters: A Highly Active Heterogeneous Catalyst for Selective Oxidation of Alcohols by Use of Molecular Oxygen. *J. Am. Chem. Soc.* **2004,** *126*, 10657-10666.

(34) Li, F.; Zhang, Q.; Wang, Y., Size dependence in solvent-free aerobic oxidation of alcohols catalyzed by zeolite-supported palladium nanoparticles. *Appl. Catal. A* **2008,** *334*, 217-226.

(35) Chen, J.; Zhang, Q.; Wang, Y.; Wan, H., Size-Dependent Catalytic Activity of Supported Palladium Nanoparticles for Aerobic Oxidation of Alcohols. *Adv. Synth. Catal.* **2008,** *350*, 453-464.

(36) Esmaeili, E.; Mortazavi, Y.; Khodadadi, A. A.; Rashidi, A. M.; Rashidzadeh, M., The role of tin-promoted Pd/MWNTs via the management of carbonaceous species in selective hydrogenation of high concentration acetylene. *Appl. Surf. Sci.* **2012,** *263*, 513-522.

(37) Zhao, J.; Xu, X.; Li, X.; Wang, J., Promotion of Sn on the Pd/AC catalyst for the selective hydrogenation of cinnamaldehyde. *Catal. Commun.* **2014,** *43*, 102-106.

(38) Vicente, A.; Lafaye, G.; Especel, C.; Marécot, P.; Williams, C. T., The relationship between the structural properties of bimetallic Pd–Sn/SiO_2 catalysts and their performance for selective citral hydrogenation. *J. Catal.* **2011,** *283*, 133-142.

(39) Mavrokefalos, C. K.; Hasan, M.; Khunsin, W.; Schmidt, M.; Maier, S. A.; Rohan, J. F.; Compton, R. G.; Foord, J. S., Electrochemically modified boron-doped diamond electrode with Pd and Pd-Sn nanoparticles for ethanol electrooxidation. *Electrochim. Acta* **2017,** *243*, 310-319.

(40) Liu, M.; Tang, W.; Xu, Y.; Yu, H.; Yin, H.; Zhao, S.; Zhou, S., Pd-SnO_2/Al_2O_3 heteroaggregate nanocatalysts for selective hydrogenations of p-nitroacetophenone and p-nitrobenzaldehyde. *Appl. Catal. A* **2018,** *549*, 273-279.

(41) Fang, W.; Chen, J.; Zhang, Q.; Deng, W.; Wang, Y., Hydrotalcite-Supported Gold Catalyst for the Oxidant-Free Dehydrogenation of Benzyl Alcohol: Studies on Support and Gold Size Effects. *Chem. Eur. J.* **2011,** *17*, 1247-1256.

(42) Chen, J.; Sun, W.; Wang, Y.; Fang, W., Performant Au hydrogenation catalyst cooperated with Cu-doped Al_2O_3 for selective conversion of furfural to furfuryl alcohol at ambient pressure. *Green Energy Environ.* **2020,** DOI: 10.1016/j.gee.2020.05.005.

(43) Wang, R.; Li, B.; Xiao, Y.; Tao, X.; Su, X.; Dong, X., Optimizing Pd and Au-Pd decorated Bi_2WO_6 ultrathin nanosheets for photocatalytic selective oxidation of aromatic alcohols. *J. Catal.* **2018,** *364*, 154-165.

(44) Zhou, W.; Li, M.; Ding, O. L.; Chan, S. H.; Zhang, L.; Xue, Y., Pd particle size effects on oxygen electrochemical reduction. *Int. J. Hydrogen Energy* **2014,** *39*, 6433-6442.

(45) Zhang, M.; Wu, S.; Bian, L.; Cao, Q.; Fang, W., One-pot synthesis of Pd-promoted Ce–Ni mixed oxides as efficient catalysts for imine production from the direct N-alkylation of amine with alcohol. *Catal. Sci. Technol.* **2019,** *9*, 286-301.

(46) Fang, W.; Fan, Z.; Shi, H.; Wang, S.; Shen, W.; Xu, H.; Clacens, J.-M.; De Campo, F.; Liebens, A.; Pera-Titus, M., Aquivion®-carbon composites via hydrothermal carbonization: amphiphilic catalysts for solvent-free biphasic acetalization. *J. Mater. Chem. A* **2016,** *4*, 4380-4385.

(47) Sun, W.; Gao, T.; Zhu, G.; Cao, Q.; Fang, W., Influence of Support Properties and Particle Size on the Gold-Catalyzed Base-Free Aerobic Oxidation of 5-Hydroxymethylfurfural. *ChemistrySelect* **2020,** *5*, 1416-1423.

(48) Zhou, J.-H.; Sui, Z.-J.; Zhu, J.; Li, P.; Chen, D.; Dai, Y.-C.; Yuan, W.-K., Characterization of surface oxygen complexes on carbon nanofibers by TPD, XPS and FT-IR. *Carbon* **2007,** *45*, 785-796.

(49) Wan, X.; Zhou, C.; Chen, J.; Deng, W.; Zhang, Q.; Yang, Y.; Wang, Y., Base-Free Aerobic Oxidation of 5-Hydroxymethyl-furfural to 2,5-Furandicarboxylic Acid in Water Catalyzed by Functionalized Carbon Nanotube-Supported Au–Pd Alloy Nanoparticles. *ACS Catal.* **2014,** *4*, 2175-2185.

(50) Wang, J.; Kondrat, S. A.; Wang, Y.; Brett, G. L.; Giles, C.; Bartley, J. K.; Lu, L.; Liu, Q.; Kiely, C. J.; Hutchings, G. J., Au–Pd Nanoparticles Dispersed on Composite Titania/Graphene Oxide-Supports as a Highly Active Oxidation Catalyst. *ACS Catal.* **2015,** *5*, 3575-3587.

(51) Cargnello, M.; Doan-Nguyen, V. V. T.; Gordon, T. R.; Diaz, R. E.; Stach, E. A.; Gorte, R. J.; Fornasiero, P.; Murray, C. B., Control of Metal Nanocrystal Size Reveals Metal-Support Interface Role for Ceria Catalysts. *Science* **2013,** *341*, 771.

(52) Zhou, W. P.; Lewera, A.; Larsen, R.; Masel, R. I.; Bagus, P. S.; Wieckowski, A., Size Effects in Electronic and Catalytic Properties of Unsupported Palladium Nanoparticles in Electrooxidation of Formic Acid. *J. Phys. Chem. B* **2006,** *110*, 13393-13398.

(53) Jiao, W.; Chen, C.; You, W.; Zhang, J.; Liu, J.; Che, R., Yolk–Shell Fe/Fe_4N@Pd/C Magnetic Nanocomposite as an Efficient Recyclable ORR Electrocatalyst and SERS Substrate. *Small* **2019,** *15*, 1805032.

(54) Liu, M.; Tang, W.; Xie, Z.; Yu, H.; Yin, H.; Xu, Y.; Zhao, S.; Zhou, S., Design of Highly Efficient Pt-SnO_2 Hydrogenation Nanocatalysts using Pt@Sn Core–Shell Nanoparticles. *ACS Catal.* **2017,** *7*, 1583-1591.

(55) Zhang, J.; Shao, Q.; Zhang, Y.; Bai, S.; Feng, Y.; Huang, X., Promoting the Direct H_2O_2 Generation Catalysis by Using Hollow Pd–Sn Intermetallic Nanoparticles. *Small* **2018,** *14*, 1703990.

(56) Wang, Y.; Lu, Y.; Cao, Q.; Fang, W., A magnetic CoRu–CoO_X nanocomposite efficiently hydrogenates furfural to furfuryl alcohol at ambient H_2 pressure in water. *Chem. Commun.* **2020,** *56*, 3765-3768.

(57) Stamenković, V. R.; Arenz, M.; Lucas, C. A.; Gallagher, M. E.; Ross, P. N.; Marković, N. M., Surface Chemistry on Bimetallic Alloy Surfaces: Adsorption of Anions and Oxidation of CO on $Pt_3Sn(111)$. *J. Am. Chem. Soc.* **2003,** *125*, 2736-2745.

(58) Wang, X.; Wu, G.; Guan, N.; Li, L., Supported Pd catalysts for solvent-free benzyl alcohol selective oxidation: Effects of calcination pretreatments and reconstruction of Pd sites. *Appl. Catal. B* **2012,** *115-116*, 7-15.

(59) Ouyang, L.; Da, G.-j.; Tian, P.-f.; Chen, T.-y.; Liang, G.-d.; Xu, J.; Han, Y.-F., Insight into active sites of Pd–Au/TiO_2 catalysts in hydrogen peroxide synthesis directly from H_2 and O_2. *J. Catal.* **2014,** *311*, 129-136.

(60) Lee, S.; Jeong, H.; Chung, Y.-M., Direct synthesis of hydrogen peroxide over Pd/C catalyst prepared by selective adsorption deposition method. *J. Catal.* **2018,** *365*, 125-137.

Table 1. Base-free aerobic oxidation of vanillyl alcohol to vanillin over supported noble metal catalysts

Entry	Catalyst	Solvent	*T* (°C)	*t* (h)	Oxidant	Conv. (%)	Select. (%)	TON	TOF	Refs.
1	Pt/CuClP	*t*-butanol	170	10	air, 20 bar	32	76	298	93	(19)
2	Au-Pd@HT-PO_4^{3-}	dioxane	25	24	air, 1 bar	53	50	81	*n.d.*	(20)
3	Pd/C-0	*p*-xylene	120	9	O_2, 5bar	100	100	532	268	this work
4	0.1Sn-Pd/C	*p*-xylene	120	6	O_2, 3bar	100	100	649	458	this work

Table 2 Catalytic performances of the 0.1Sn-Pd/C catalyst for base-free aerobic oxidation of various primary alcohols

Entry	Alcohol	*t* (h)	Conv. (%)	Select. (%)[a]	TON[b]
1	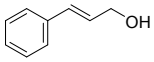	9	100	100	649
2	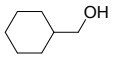	12	98	100	636
3	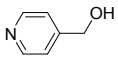	12	96	100	623
4	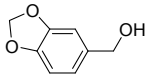	18	78	99	501
5	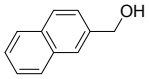	18	67	99	431
6	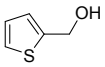	24	33	99	212
7	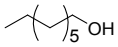	24	46	85	254

Reaction conditions: alcohol, 1 mmol; 0.1Sn-Pd/C catalyst, 15 mg; *p*-xylene, 10 mL; O_2, 1 bar; temperature: 60 °C. [a] Selectivity of the corresponding aldehyde is calculated based on the carbon balance. [b] Total turnover number (TON) = $mol._{aldehyde}/mol._{(Pd+Sn)}$

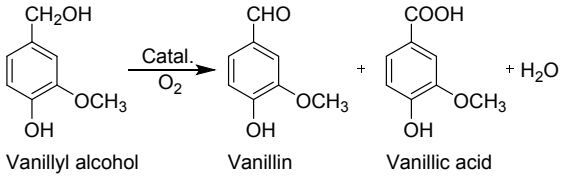

Scheme 1 Products from catalytic aerobic oxidation of vanillyl alcohol.

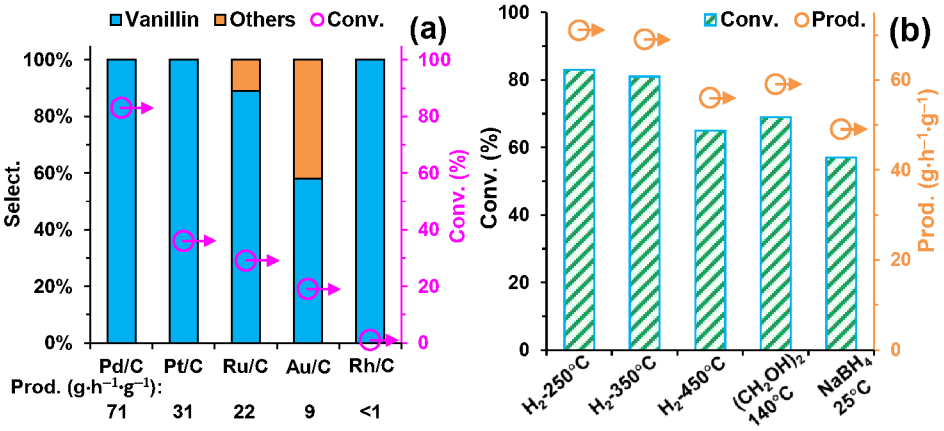

Figure 1. (a) Catalytic performances of activated charcoal supported noble metals for base-free aerobic oxidation of vanillyl alcohol to vanillin. Reaction conditions: vanillyl alcohol, 1 mmol; catalyst, 20 mg; *p*-xylene, 10 mL; O_2, 5 bar; temperature: 120 °C; time, 9 h. (b) Catalytic performances of Pd/C-25 catalysts pre-reduced by different methods for base-free aerobic oxidation of vanillyl alcohol to vanillin. Reaction conditions: vanillyl alcohol, 1 mmol; Pd/C-25 catalyst, 20 mg; *p*-xylene, 10 mL; O_2, 5 bar; temperature: 120 °C; time, 9 h.

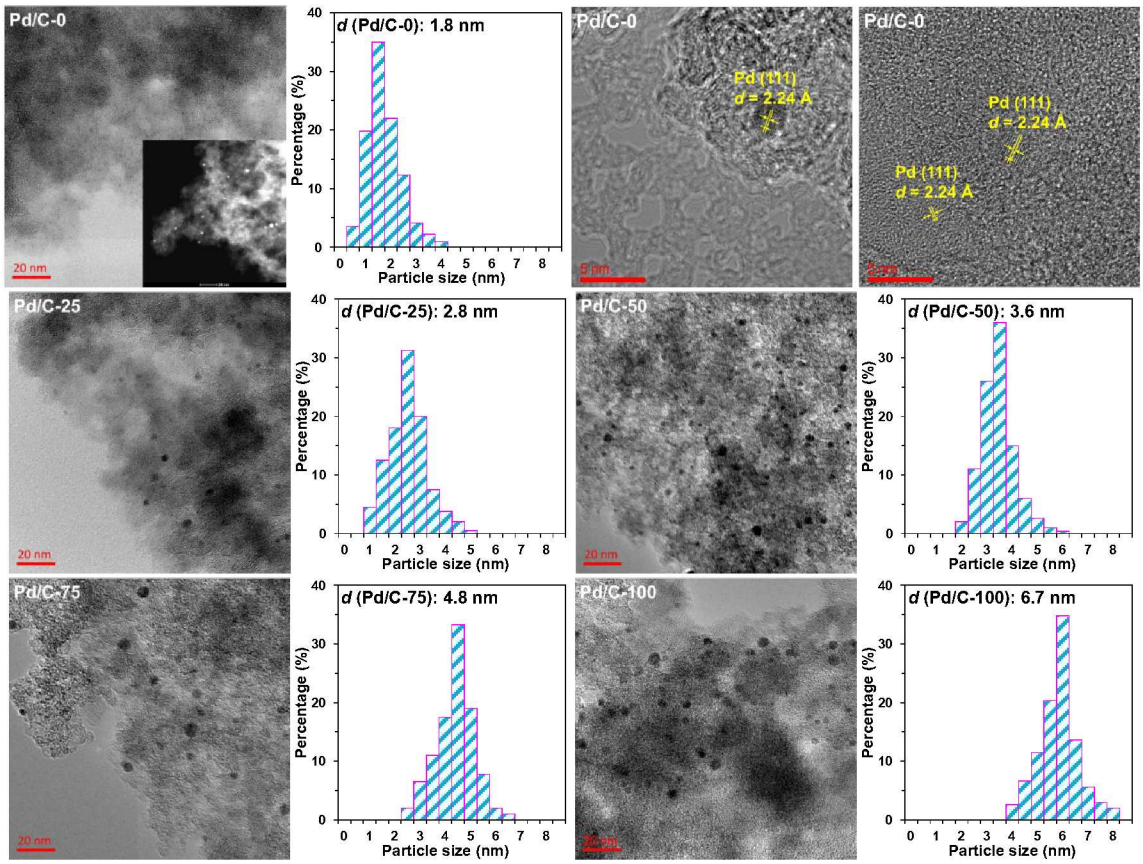

Figure 2. TEM images, the corresponding size distribution and the mean particle size of Pd nanoparticles for Pd/C catalysts prepared at different temperatures. HAADF-STEM image and high resolution TEM images from different regions are additionally provided for the Pd/C-0 catalyst.

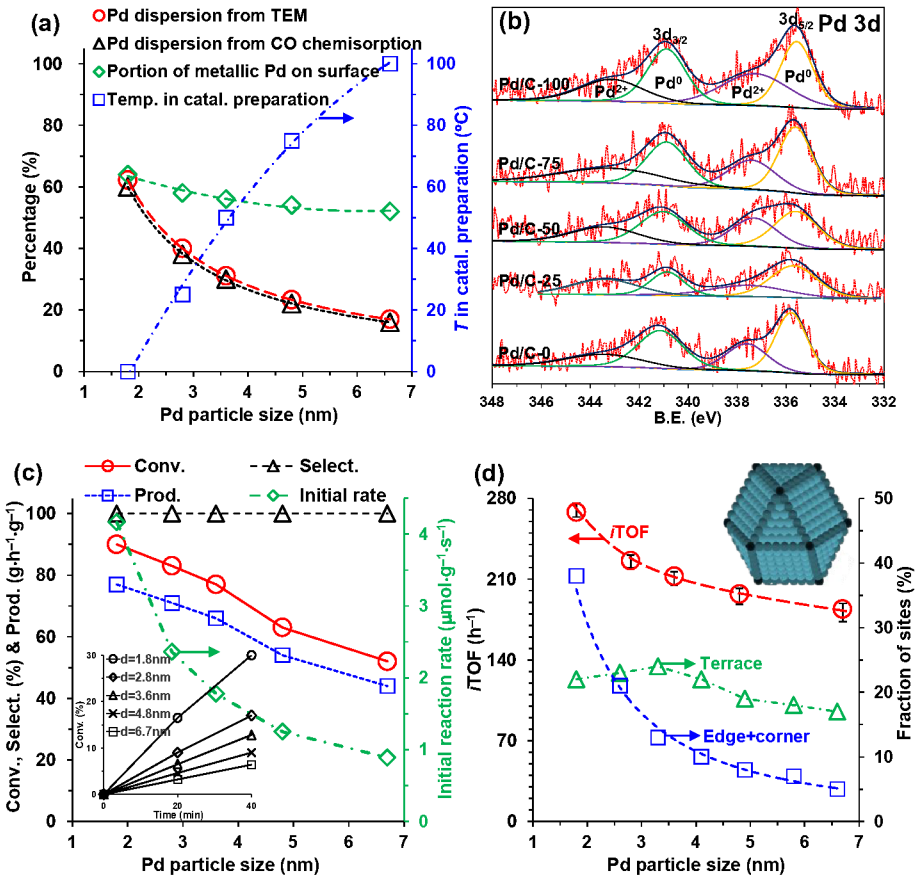

Figure 3. (a) Dependence of Pd mean particle size, Pd dispersion and portion of metallic Pd on surface on the temperature used in Pd/C catalyst preparation. (b) Deconvoluted XPS spectra of Pd 3d core level for Pd/C catalysts prepared at different temperatures. (c) Catalytic performances and initial reaction rates of Pd/C catalysts with different Pd particle sizes for base-free aerobic oxidation of vanillyl alcohol to vanillin. Reaction conditions: vanillyl alcohol, 1 mmol; Pd/C catalyst, 20 mg; *p*-xylene, 10 mL; O_2, 5 bar; temperature: 120 °C; time, 1 h or 9 h. (d) Dependence of *i*TOF , the fraction of terrace, edge and corner Pd atoms on Pd particles size in a truncated cubo-octahedral geometry on Pd particle size.

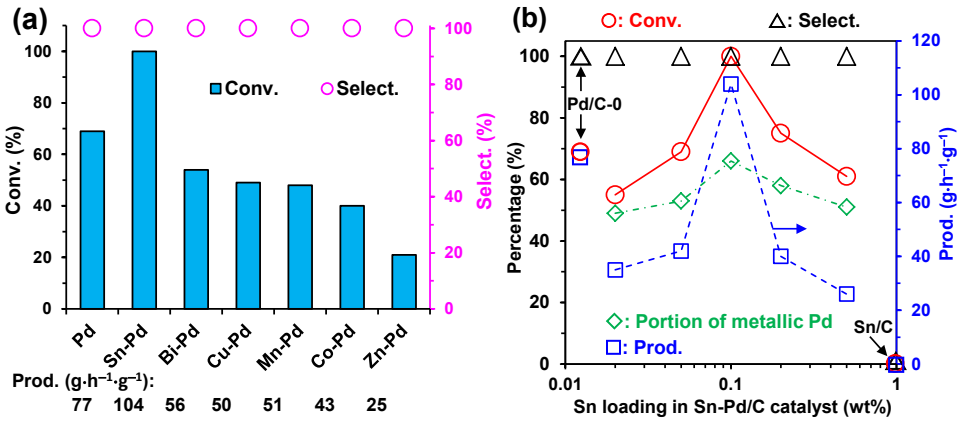

Figure 4. (a) Catalytic performances of different metals promoted Pd/C-0 catalysts for aerobic oxidation of vanillyl alcohol to vanillin. Reaction conditions: vanillyl alcohol, 1 mmol; catalyst, 15 mg; *p*-xylene, 10 mL; O_2, 5 bar; temperature: 120 °C; time, 9 h. (b) Catalytic performances of *y*Sn-Pd/C, Pd/C-0 and Sn/C catalysts for base fee aerobic oxidation of vanillyl alcohol to vanillin. Reaction conditions: vanillyl alcohol, 1 mmol; catalyst, 15 mg; *p*-xylene, 10 mL; O_2, 5 bar; temperature: 120 °C; time, 9 h.

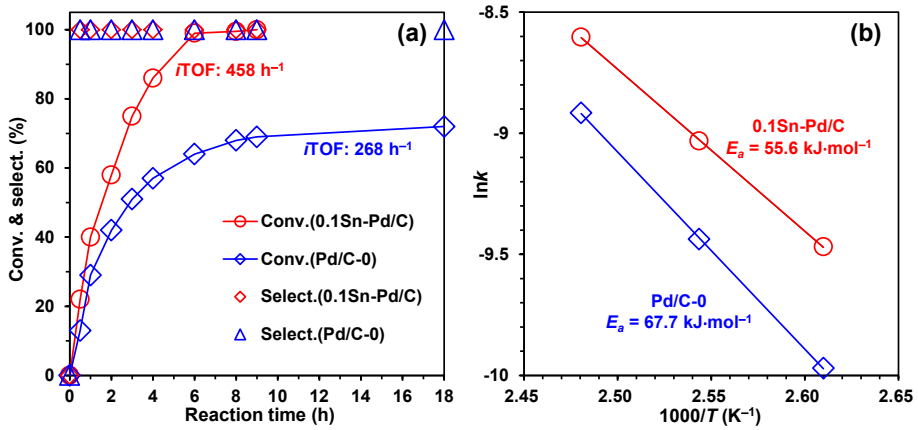

Figure 5. (a) Time course curves and (b) apparent activation energy (E_a) obtained on the Pd/C-0 and 0.1Sn-Pd/C catalysts for base-free aerobic oxidation of vanillyl alcohol to vanillin. Reaction conditions: vanillyl alcohol, 1 mmol; catalyst, 15 mg; *p*-xylene, 10 mL; O_2, 3 bar; temperature: 110–130 °C (a); time, 9 h (b).

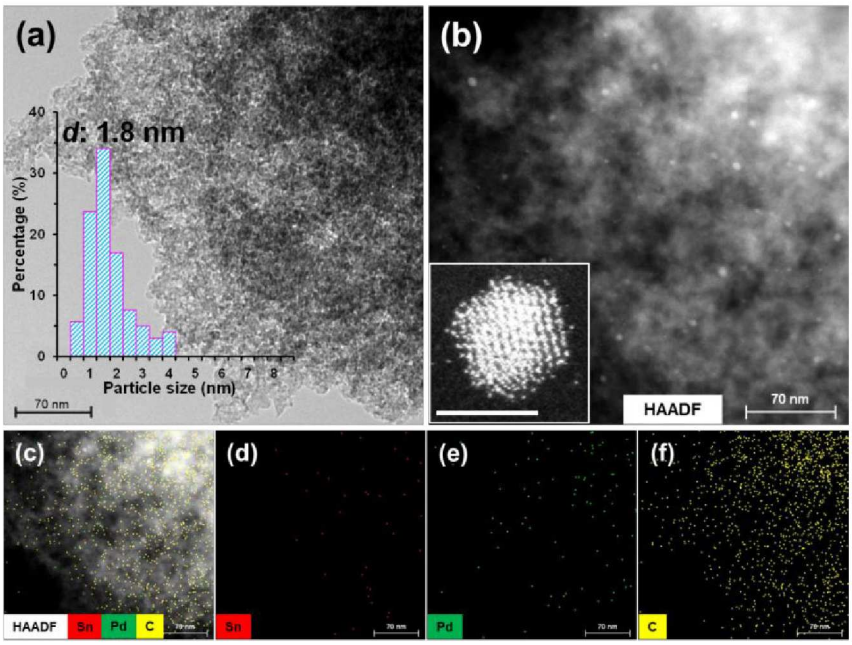

Figure 6. (a) Bright-field STEM image with insertion of corresponding size distribution of Pd nanoparticles and (b) HAADF-STEM image with insertion of the atomic resolution image (scale bar: 2 nm) for a representative Pd nanoparticle of the 0.1Sn-Pd/C catalyst. (c-f) Color-coded EDS elemental maps of Sn (red), Pd (green) and C (yellow).

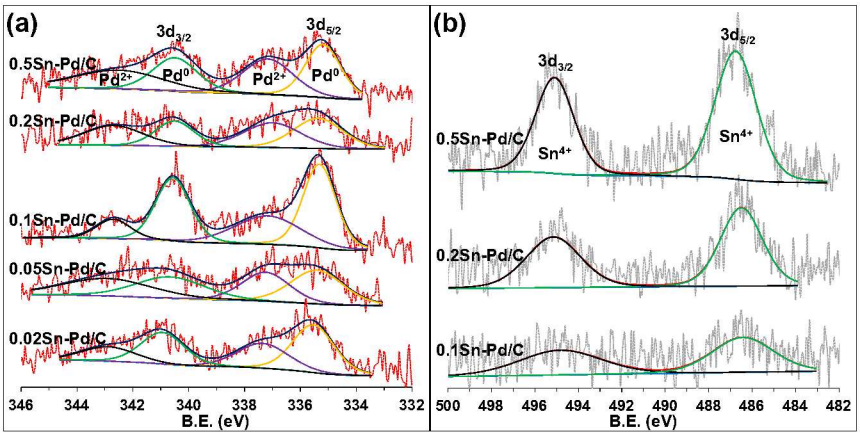

Figure 7. Deconvoluted XPS spectra of (a) Pd 3d and (b) Sn 3d core levels for *y*Sn-Pd/C catalysts.

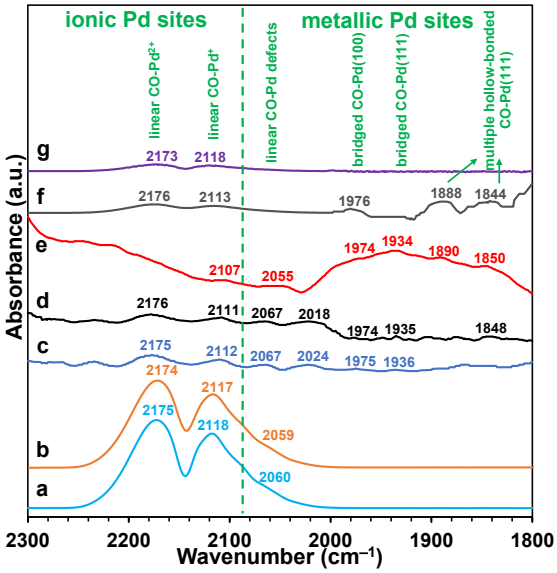

Figure 8. *in situ* DRIFT-IR spectra of CO adsorption for (a) Pd/C-0 unreduced, (b) 0.1Sn-Pd/C unreduced, (c–g) Pd/C-0, 0.02Sn-Pd/C, 0.1Sn-Pd/C, 0.2Sn-Pd/C and 0.5Sn-Pd/C reduced with H_2 at 250 °C.

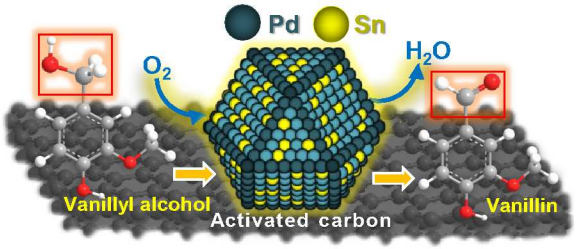

Graphical abstract

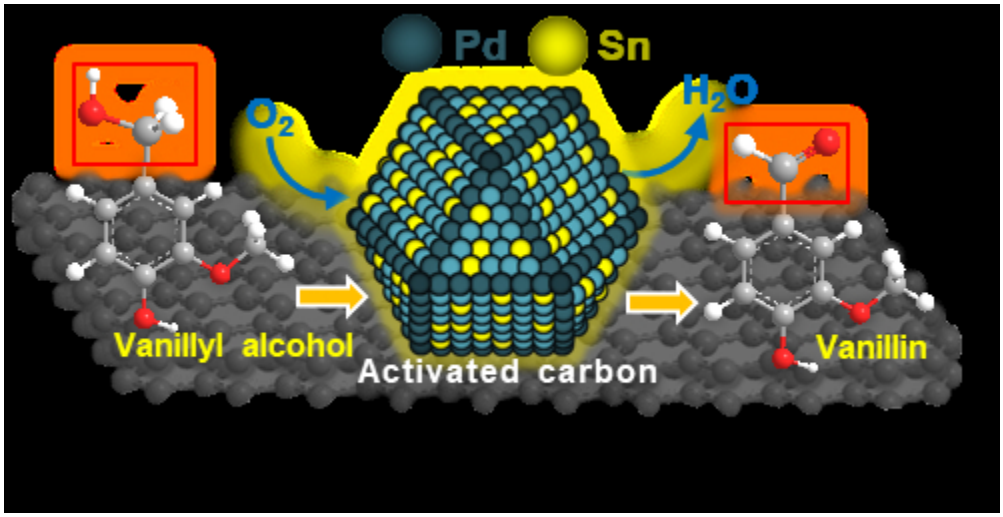

TOC graphic

84x43mm (150 x 150 DPI)

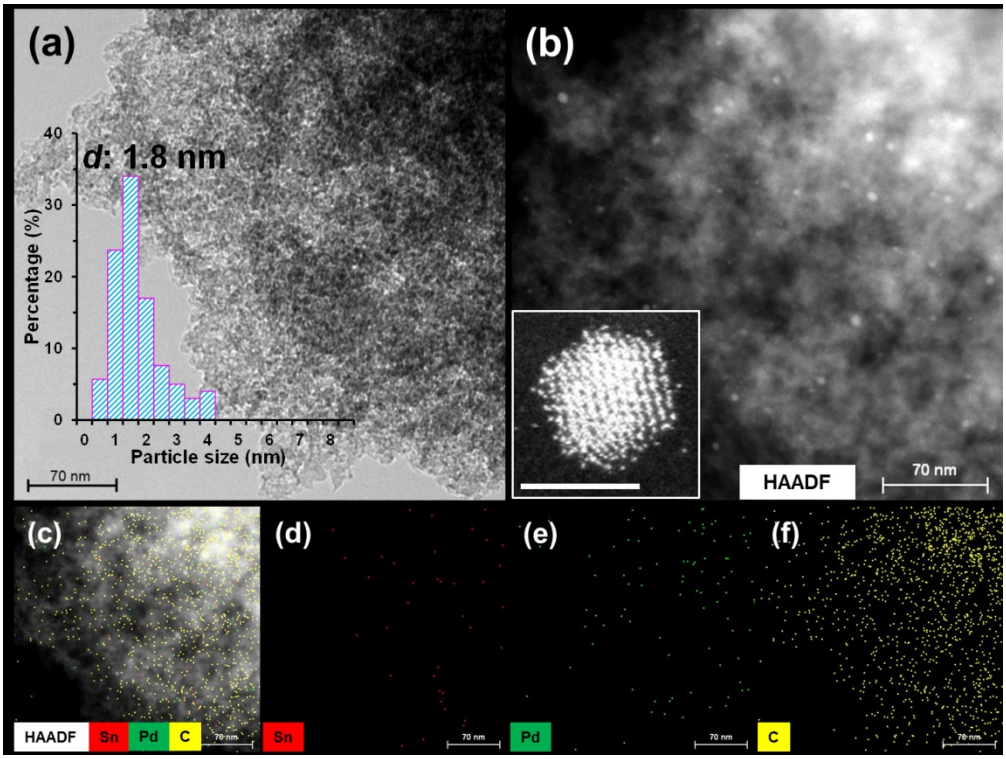

Figure 6

244x183mm (150 x 150 DPI)